AMERICAN SOCIETY FOR MICROBIOLOGY | Molecular and Cellular Biology

Claudin-21 Has a Paracellular Channel Role at Tight Junctions

Hiroo Tanaka,[a] Yasuko Yamamoto,[b] Hiroka Kashihara,[a] Yuji Yamazaki,[c] Kazutoshi Tani,[d] Yoshinori Fujiyoshi,[d,e] Katsuhiko Mineta,[f] Kosei Takeuchi,[g] Atsushi Tamura,[a] Sachiko Tsukita[a]

Graduate School of Medicine/Frontier Bioscience, Osaka University, Suita, Osaka, Japan[a]; Graduate School of Medicine, Kyoto University, Kyoto, Japan[b]; Lewis-Sigler Institute for Integrative Genomics, Princeton University, Princeton, New Jersey, USA[c]; Cellular and Structural Physiology Institute (CeSPI), Nagoya University, Nagoya, Japan[d]; Department of Basic Medical Science, Graduate School of Pharmaceutical Science, Nagoya University, Nagoya, Japan[e]; Computational Bioscience Research Center, King Abdullah University of Science and Technology (KAUST), Thuwal, Kingdom of Saudi Arabia[f]; Department of Biology, School of Medicine, Aichi Medical University, Nagakute, Aichi, Japan[g]

Claudin protein family members, of which there are at least 27 in humans and mice, polymerize to form tight junctions (TJs) between epithelial cells, in a tissue- and developmental stage-specific manner. Claudins have a paracellular barrier function. In addition, certain claudins function as paracellular channels for small ions and/or solutes by forming selective pores at the TJs, although the specific claudins involved and their functional mechanisms are still in question. Here we show for the first time that claudin-21, which is more highly expressed in the embryonic than the postnatal stages, acts as a paracellular channel for small cations, such as Na^+, similar to the typical channel-type claudins claudin-2 and -15. Claudin-21 also allows the paracellular passage of larger solutes. Our findings suggest that claudin-21-based TJs allow the passage of small and larger solutes by both paracellular channel-based and some additional mechanisms.

Epithelial cell sheets form and cover every compartment of the body. Homeostasis is specifically maintained for organ and tissue function in each compartment. To create sheets with a barrier function, epithelial cells adhere to each other side by side through well-organized cell-cell adhesion systems (1), such as tight junctions (TJs), which maintain distinct environments by blocking the free exchange of molecules across the cell sheet (2, 3). Accumulating evidence indicates that the molecular strands that form the TJ barriers are composed primarily of polymerized claudins, which are adhesion molecules containing four transmembrane helices (2, 4). The claudins both create the paracellular barrier and determine which ions and/or molecules can selectively cross it (5–7).

The claudins comprise a large gene family with at least 27 members, in humans or mice, that have distinct expression patterns and properties (2, 3, 8). Epithelial cells generally express multiple types of claudins; the particular claudin combination expressed appears to determine the specific properties of each TJ-based paracellular permselective barrier (9–22). Two categories of claudins have been proposed, namely, the paracellular barrier type and the paracellular channel type, based on the transepithelial electrical resistance (TER) or on the cation and/or anion permeability of many epithelial cell lines (5, 7). Among some claudins characterized as channel-type claudins, such as claudin-2, -7, -10, -15, -16, and -17, claudin-2 and -15 have been studied extensively with respect to specific ions and water (9–11, 14, 17, 20, 21, 23, 24).

The structure of claudin-15 was recently analyzed; this analysis revealed that two extracellular segments form a unique β sheet domain fixed to a transmembrane four-helix bundle by a W-LW claudin consensus motif (25, 26). The high-resolution structure of claudin-15 suggests that a β-barrel pore created by eight claudin molecules in the region between two cells can form a paracellular channel, which is regulated by charged residues on the claudins' extracellular domains.

Although potential mechanisms have been reported for claudins' paracellular barrier function and channel activity for small ions and/or solutes, how relatively large solutes occasionally pass through TJs is still unknown (7, 19). Since the paracellular passage of large solutes is detected physiologically as a temperature-dependent and nonrestrictive permeability (7, 27, 28), it is likely that changes in the dynamics of claudin-based TJ strands that result in gaps are involved (7, 19, 29). However, no information on such large, temperature-dependent paracellular gaps has been reported, and there is little evidence that any specific claudin is involved in this phenomenon.

Here we found that claudin-21, which is more highly expressed in the embryonic than the postnatal stages (8), functions as a paracellular channel for small cations (diameter < 5 Å) and allows the paracellular passage of larger solutes (diameter > 5 Å). Furthermore, these claudin-21-based paracellular permeabilities have temperature-dependent characteristics, similar to the case for claudin-15. The size- and temperature-dependent paracellular permeabilities based on claudin-21 may involve two dynamically regulated paracellular pathways: one that is based on paracellular channels and another that is unknown. This variation in claudin-21's paracellular function may be involved in optimizing a biological system's microenvironment. Further studies of channel-type claudins will increase our understanding of epithe-

Received 5 August 2015 **Returned for modification** 16 September 2015
Accepted 25 December 2015

Accepted manuscript posted online 4 January 2016

Citation Tanaka H, Yamamoto Y, Kashihara H, Yamazaki Y, Tani K, Fujiyoshi Y, Mineta K, Takeuchi K, Tamura A, Tsukita S. 2016. Claudin-21 has a paracellular channel role at tight junctions. Mol Cell Biol 36:954–964. doi:10.1128/MCB.00758-15.

Address correspondence to Atsushi Tamura, atamura@biosci.med.osaka-u.ac.jp, or Sachiko Tsukita, atsukita@biosci.med.osaka-u.ac.jp.

H. Tanaka, Y. Yamamoto, and H. Kashihara contributed equally to this article.

Supplemental material for this article may be found at http://dx.doi.org/10.1128/MCB.00758-15.

lial barriers and reveal new therapeutic avenues for treating barrier-related diseases.

MATERIALS AND METHODS

Plasmids and antibodies. Full-length mouse claudin-2, -15, and -21 cDNAs were subcloned into an N-terminally Venus-tagged CAGGS expression vector. Rat anti-E-cadherin monoclonal antibody (MAb) was a kind gift from Masatoshi Takeichi (Riken CDB, Japan). Rat anti-ZO-1 MAbs and rabbit anti-green fluorescent protein (anti-GFP) polyclonal antibodies (pAbs) were described previously (8). Rabbit anti-claudin-1, -3, -4, and -7 pAbs and mouse anti-α-tubulin MAb were purchased from Invitrogen. A rabbit anti-claudin-2 pAb was purchased from Immuno-Biological Laboratories Co., Ltd. (Gumma, Japan). The rabbit anti-claudin-15 pAb was described previously (17). A rabbit anti-glyceraldehyde-3-phosphate dehydrogenase (anti-GAPDH) pAb was purchased from Sigma-Aldrich Japan (Tokyo, Japan). A polypeptide with the sequence DGSSSW MADADATQACAPVEEEFDGSFHLTPRPVNQVI, corresponding to the COOH-terminal cytoplasmic region of mouse claudin-21, was synthesized and coupled via cysteine to keyhole limpet hemocyanin. This conjugated peptide was used as an antigen to immunize rabbits and raise a pAb against claudin-21. Primers and probes used for probe-based quantitative real-time PCR were designed by and purchased from Integrated DNA Technologies, Inc. (Coralville, IA). The primer and probe sequences were as follows: probe for claudin-21, 5′-6-carboxyfluorescein (FAM)-TCTAGCTGC-ZEN-GGGTTGGAATGCTT-IABkFQ-3′; forward primer for claudin-21, 5′-CTGGGACTATTGGGACTTCTG-3′; reverse primer for claudin-21, 5′-AGGAGACTGGAAAGAGGGTAG-3′; probe for GAPDH, 5′-FAM-TGCAAATGG-ZEN-CAGCCCTGGTG-IABkFQ-3′; forward primer for GAPDH, 5′-GTGGAGTCATACTGGAACATGTAG-3′; and reverse primer for GAPDH, 5′-AATGGTGAAGGTCGGTGTG-3′.

Cell culture and transfection. MDCK I, MDCK II, or EpH4 cells were cultured in Dulbecco's modified Eagle's medium (DMEM) supplemented with 10% fetal calf serum (FCS). Transfection was performed using Lipofectamine Plus or Lipofectamine 2000 (Life Technologies Japan Ltd., Tokyo, Japan) following the manufacturer's instructions. To establish stable transfectants, the transfected cells were selected by incubation in medium containing 500 μg/ml G418 (Nacalai Tesque, Kyoto, Japan), and clones derived from single cells were picked up.

Immunoblotting. To prepare total cell lysates of MDCK I, MDCK II, EpH4, and Venus-tagged claudin-expressing transfected MDCK I cells, epithelial cells were washed with solution A (120 mM NaCl, 10 mM $NaHCO_3$, 5 mM KCl, 1.2 mM $CaCl_2$, 1.0 mM $MgCl_2$, and 10 mM Tris-HEPES, pH 7.4) and then lysed with SDS-PAGE sample buffer, sonicated, and boiled. Constant amounts of protein samples were separated by SDS-PAGE, transferred to a polyvinylidene difluoride (PVDF) membrane, and probed with appropriate antibodies. Signals were acquired by using an Image Quant LAS 4000 instrument (GE Healthcare, Tokyo, Japan).

Immunofluorescence microscopy. MDCK I transfectants plated on glass coverslips were fixed with ice-cold methanol for 5 min. After being soaked in phosphate-buffered saline (PBS) containing 1% bovine serum albumin (BSA), the samples were treated with primary antibodies for 60 min at room temperature. They were then washed three times with PBS, followed by incubation for 60 min with the appropriate secondary antibodies. The samples were washed with PBS three times and then embedded in mounting medium (Dako Japan Inc., Tokyo, Japan), and the specimens were observed with a confocal laser scanning microscope (LSM710; Carl Zeiss Japan, Tokyo, Japan) equipped with a 40×, 1.2-numerical-aperture (NA) lens, with appropriate binning of pixels and exposure time. Photographs were recorded with a cooled charge-coupled device camera (Axio Cam; Carl Zeiss Japan, Tokyo, Japan). The images were analyzed with ZEN software (Carl Zeiss Japan, Tokyo, Japan). The testes and epididymides from embryonic day 18 (E18) and adult mice were embedded in OCT compound (Sakura Finetek Japan Co., Ltd., Tokyo, Japan) and frozen in liquid N_2. The frozen samples were then cut into approximately 4-μm-thick sections and allowed to dry for 30 min. They were then fixed for 5 min in ice-cold methanol. The fixed sections were stained with the appropriate antibodies or normal rabbit serum, and the specimens were observed with a confocal laser scanning microscope (LSM710; Carl Zeiss Japan, Tokyo, Japan) equipped with a 40×, 1.2-NA lens, with appropriate binning of pixels and exposure time. Photographs were recorded with a cooled charge-coupled device camera (Axio Cam; Carl Zeiss Japan, Tokyo, Japan). The images were analyzed with ZEN software (Carl Zeiss Japan, Tokyo, Japan). MDCK I transfectants plated on glass coverslips were fixed with ice-cold methanol for 5 min. After being soaked in PBS containing 1% BSA, the samples were treated with primary antibodies for 60 min at room temperature. They were then washed three times with PBS, followed by incubation for 60 min with the appropriate secondary antibodies. The samples were washed with PBS three times, embedded in mounting medium (Dako Japan Inc., Tokyo, Japan), and observed by fluorescence microscopy (Olympus, Tokyo, Japan). The images were analyzed with MetaMorph (Molecular Devices Japan, Tokyo, Japan).

Measurement of TER. For the TER measurements, 1×10^5 cells were plated on 12-mm-diameter Transwell filters, and the culture medium was exchanged every day. TER was measured directly in the culture medium by using a Millicell-ERS epithelial volt-ohmmeter (Merck Millipore, Darmstadt, Germany). The TER values were calculated by subtracting the background TER of blank filters and multiplying the result by the surface area of the filter. The TER values reached a maximum by 6 days under these experimental conditions.

Electrophysiology. The electrophysiological characterization of MDCK I cell monolayers was carried out according to published methods (30, 31). Venus-claudin-expressing transfectants of MDCK I cells were grown on Transwell filters (Costar; Corning Life Sciences, Acton, MA) for 7 days. To examine the transepithelial conductance, cell layers were mounted in Ussing chambers. Each chamber was filled with 5 ml of solution (150 mM NaCl, 2 mM $CaCl_2$, 1 mM $MgCl_2$, 10 mM mannitol, and 10 mM Tris-HEPES, pH 7.4), and the temperature of the solution was maintained at 37°C, 26°C, 15°C, or 4°C. The solution in chambers was bubbled with 100% O_2 continuously. The transepithelial potential was measured through 3 M KCl-agar bridges connected to calomel electrodes by use of a voltage-clamping device (Nihon Kohden, Tokyo, Japan). To determine the NaCl dilution potential, the basal solution was replaced with one containing 75 mM NaCl instead of 150 mM NaCl (osmolarity was maintained by use of mannitol). To measure the permeability for organic cations, the basolateral medium was changed to a solution containing 75 mM organic cation chloride salt and 75 mM NaCl. The organic cations included methylammonium (MA), ethylammonium (EA), tetramethylammonium (TMA), tetraethylammonium (TEA), arginine (Arg), and *N*-methyl-D-glucamine (NMDG). The NaCl dilution potential and bionic potential were measured as described previously (31). The transepithelial conductance was calculated by passing a current and measuring the potential across the epithelial cell sheet according to Ohm's law. The current was applied across the epithelial cell sheet through a pair of Ag/$AgCl_2$ electrodes that were kept in contact with the bathing solutions via a pair of 1 M NaCl-agar bridges. The potential was compensated for by the resistance of the solution between the potential-measuring salt bridges.

The resulting potential was corrected for the liquid junction potential, which was determined by performing analogous experiments using the method described by Alan Yu's group (31).

Estimation of the paracellular channel capacity and pore size of claudin-21 and -15. To estimate the paracellular channel capacity, the transepithelial permeability for cations (Na^+, MA^+, EA^+, TMA^+, TEA^+, Arg^+, and $NMDG^+$) of MDCK I-Venus cells, MDCK I-Venus-claudin-21 cells, or MDCK I-Venus-claudin-15 cells at 4°C was determined as described above. To estimate the pore size of claudin-21 or -15, the transepithelial permeability of MDCK I-Venus cells for various cations at 4°C was subtracted from that of MDCK I-Venus-claudin-21 cells or MDCK I-Venus-claudin-15 cells at 4°C. The resulting permeabilities were plotted

as a function of cation diameter. The pore size of claudin-21 or -15 was deduced from the graph.

Estimation of temperature-dependent paracellular pathway capacity and its size exclusion threshold. To estimate the capacity of the temperature-dependent paracellular pathway, the transepithelial permeability for cations (Na^+, MA^+, EA^+, TMA^+, TEA^+, Arg^+, and $NMDG^+$) of MDCK I-Venus, MDCK I-Venus-claudin-21, or MDCK I-Venus-claudin-15 cells at 4°C was subtracted from that of MDCK I-Venus, MDCK I-Venus-claudin-21, or MDCK I-Venus-claudin-15 cells at 37°C, and the result is referred to here as "cation permeability (37°C − 4°C)." To estimate the size exclusion threshold of the temperature-dependent permeability, the cation permeability (37°C − 4°C) of MDCK I-Venus cells was subtracted from that of MDCK I-Venus-claudin-21 cells or MDCK I-Venus-claudin-15 cells. The resulting permeabilities were plotted as a function of the cation diameter. The size exclusion threshold of the temperature-dependent permeability due to claudin-21 or -15 was deduced from the graph.

Probe-based qRT-PCR. The primers and probes used to detect the expression of mouse claudin-21 and mouse GAPDH genes were purchased from Integrated DNA Technologies, Inc. (Coralville, IA). The sequences of the primers and probes are described in "Plasmids and antibodies" above. Template cDNAs from several tissues of E18.5 and adult C57BL/6 mice were purchased from Genostaff Co., Ltd., Tokyo, Japan. Thunderbird probe qPCR mix (Toyobo Co., Ltd., Osaka, Japan) was used as the PCR reagent. Probe-based quantitative real-time reverse transcription-PCR (qRT-PCR) was performed with a ViiA7 real-time PCR system (Applied Biosystems Japan Ltd., Tokyo, Japan) under the following conditions: 94°C for 2 min followed by 40 cycles of 95°C for 15 s and 60°C for 1 min. The resulting data were analyzed using ViiA7 HRM software (Applied Biosystems Japan Ltd., Tokyo, Japan).

3′ rapid amplification of cDNA ends (3′RACE). Total RNA was extracted from mouse tissues. The RT-oligo-dT primer used for reverse transcription is shown in Table S1 in the supplemental material. A partial fragment of claudin-21 was amplified using the claudin-21 F1 and 3′RACE reverse primers shown in Table S1.

To perform the multiple-sequence alignment analysis, claudin-21's genomic region sequence was retrieved from the GenBank database (accession no. NG_020884). Multiple-sequence alignment was performed using the ClustalW program (32).

Homology modeling of claudins for structural analysis. The multiple-sequence alignment of mouse claudin-2, -10a, and -21 for homology modeling was performed using the ClustalW program (32). After manually modifying the alignment, homology models for claudins were built with MODELLER software v9.12 (33), using the atomic coordinates of mouse claudin-15 as a starting template, with disulfide bond restraint. The disordered regions of claudin-15 were manually removed using COOT software (34). The final model was further refined by using CNS v1.3 (35) without experimental data. The surface distribution of the electrostatic potential was calculated using Adaptive Poisson-Boltzmann Solver (APBS) (36). All structural figures were prepared using PyMOL (http://www.pymol.org/).

Animal experiments. All animal experiments were performed in accordance with protocols approved by the Osaka University School of Medicine Animal Studies Committee.

Statistical analysis. Results are expressed as means ± standard errors of the means (SEM). The statistical significance of the difference between 2 sets of data was evaluated by Student's *t* test. *P* values of <0.05 were considered statistically significant.

RESULTS

Claudin-21 nomenclature. The claudin family has at least 27 members in humans and mice, according to PSI-BLAST searches (8), and its nomenclature has been clarified (8, 37). Claudin-21 was previously called claudin-24 (38) or claudin-25 in the NCBI database. Here we use the latest nomenclature for this molecule, designating it claudin-21 (8).

Establishment of MDCK I cell monolayer exogenously expressing claudin-21. We first examined the endogenous protein expression of claudin-21 in the major cultured epithelial cell lines, such as MDCK I, MDCK II, and EpH4, using an anti-claudin-21 antibody that specifically reacts with claudin-21 (see Fig. S1 in the supplemental material). We did not detect endogenous claudin-21 protein in any of these cell lines (see Fig. S2). Next, to characterize claudin-21, we established several clones of Venus-tagged mouse claudin-21 stably transfected MDCK I cells (MDCK I-Venus-claudin-21) and mock-transfected MDCK I cells (MDCK I-Venus) (see Fig. S3A), because MDCK I cells show a prominent paracellular barrier activity (9). Venus-claudin-21 was localized to the lateral membranes of MDCK I-Venus-claudin-21 cells and colocalized with a TJ marker, ZO-1 (Fig. 1A; see Fig. S4A), although endogenous claudin-21 localization in MDCK I cells was not detected by immunofluorescence assay (Fig. 1A). These data showed that exogenous claudin-21 was integrated into the TJs as a component of the claudin strands.

Electrophysiological characterization of claudin-21 as a paracellular channel-type claudin. To unravel the functions of claudin-21 at the TJs in paracellular permeability, which is correlated with the TER, we first analyzed the TER in MDCK I-Venus-claudin-21 and MDCK I-Venus cells every day for 1 week. In the MDCK I-Venus cells, the TER increased due to the maturation of a cell sheet with a paracellular barrier. In contrast, the TER did not increase in the MDCK I-Venus-claudin-21 cells (Fig. 2A, panel a), suggesting the possibility that claudin-21 played a role as a paracellular channel. To characterize claudin-21 in more detail, we used three independent claudin-21-expressing clones in the following experiments. First, we found by immunoblotting and/or immunofluorescence assay that exogenous claudin-21 expression did not alter the levels of endogenous claudin-1, -3, -4, and -7 (see Fig. S3 in the supplemental material) or those of the other channel-type claudins, claudin-2 and -15 (see Fig. S5).

Next, to examine the ion permeability of the claudin-21-expressing transfectants, we performed detailed electrophysiological measurements by using an Ussing chamber assay. The Na^+ permeability (PNa), calculated from the conductance and dilution potential, was 1.2×10^{-6} cm/s for MDCK I-Venus cells and 11.4×10^{-6} cm/s for MDCK I-Venus-claudin-21 cells (Fig. 2A, panel b). On the other hand, the Cl^- permeability (PCl) was not significantly increased (Fig. 2A, panel b).

We next measured the permeabilities for variously sized small cations and found that the permeabilities for monocations were significantly increased in MDCK I-Venus-claudin-21 cells compared to MDCK I-Venus cells (Fig. 2A, panel c). Taken together, these data indicate that claudin-21 contributes a cationic selectivity to the paracellular permeability. These results suggest that claudin-21 functions as a paracellular channel for small cations, similar to the typical channel-type claudins claudin-2 and -15.

Next, to characterize the size dependency of the claudin-21-based paracellular permeability, we assessed the passage of larger cations, such as methylammonium (MA^+), ethylammonium (EA^+), tetramethylammonium (TMA^+), tetraethylammonium (TEA^+), arginine (Arg^+), and *N*-methyl-D-glucamine ($NMDG^+$), across MDCK I-Venus and MDCK I-Venus-claudin-21 cell sheets. There were significant increases in the permeabilities for MA^+, EA^+, TMA^+, TEA^+, Arg^+, and $NMDG^+$ across

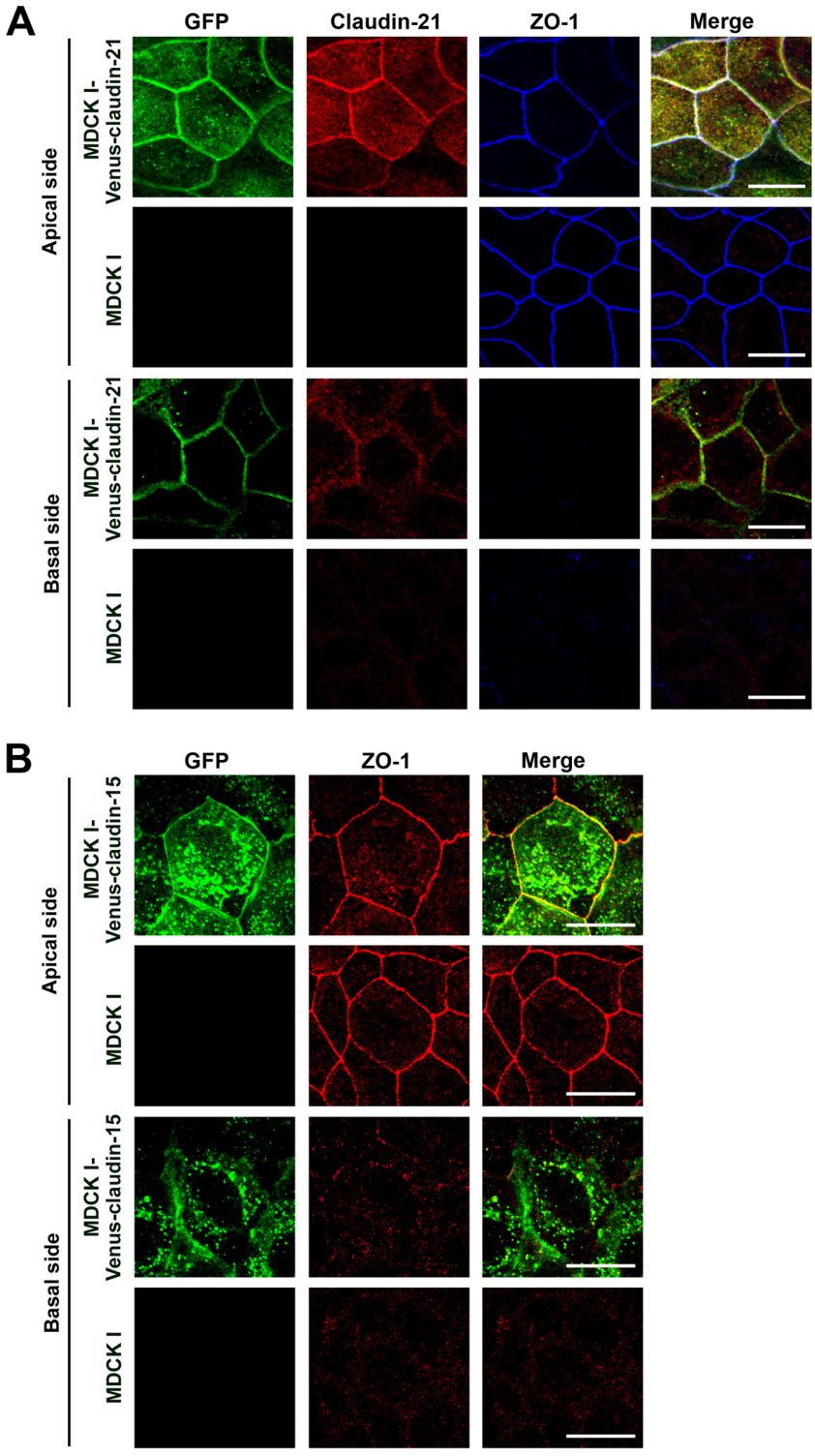

FIG 1 Mouse claudin-21 localization in MDCK I transfectant clones. (A) MDCK I cells or Venus-claudin-21-expressing transfected MDCK I cells (MDCK I-Venus-claudin-21 cells) were cultured to confluence on glass coverslips and examined by confocal laser scanning microscopy. The cells were triple stained with an anti-GFP pAb, an anti-claudin-21 pAb, and an anti-ZO-1 MAb. The anti-GFP-positive signals overlapped the anti-claudin-21-positive signals and the anti-ZO-1-positive signals. Stacked images of the apical or basal side of the epithelial cells are shown. Green, GFP; red, claudin-21; blue, ZO-1. Bars, 10 μm. (B) MDCK I cells or Venus-claudin-15-expressing transfected MDCK I cells (MDCK I-Venus-claudin-15 cells) were cultured to confluence on glass coverslips and examined by confocal laser scanning microscopy. The cells were stained with an anti-GFP pAb and an anti-ZO-1 MAb. The anti-GFP-positive signals overlapped the anti-ZO-1-positive signals. Stacked images of the apical or basal side of the epithelial cells are shown. Green, GFP; red, ZO-1. Bars, 10 μm.

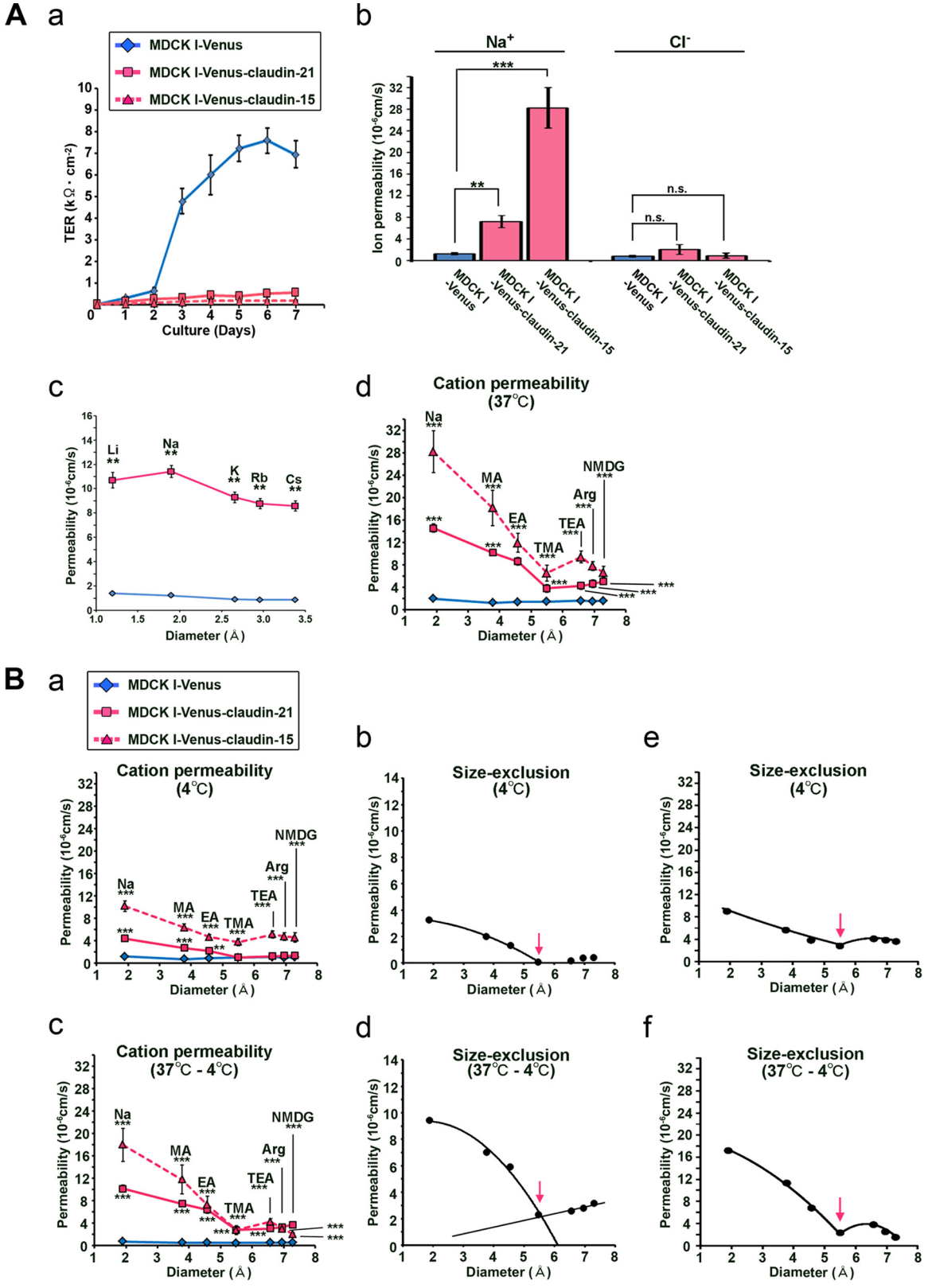

FIG 2 Physiological analyses of exogenous claudin-21-expressing MDCK I cells. (A) (a) Measurement of transepithelial electric resistance in mock-transfected MDCK I cells (MDCK I-Venus), Venus-claudin-21-expressing transfected MDCK I cells (MDCK I-Venus-claudin-21), and Venus-claudin-15-expressing transfected MDCK I cells (MDCK I-Venus-claudin-15) (n = 3/group). (b) Transepithelial ion permeabilities for Na^+ and Cl^- of MDCK I-Venus, MDCK I-Venus-claudin-21, and MDCK I-Venus-claudin-15 cells (n = 4/group). n.s., not significant; **, $P < 0.01$; ***, $P < 0.001$. (c) Monovalent cation transepithelial permeabilities of MDCK I-Venus and MDCK I-Venus-claudin-21 cells (n = 4/group). **, $P < 0.01$. (d) Transepithelial ion permeabilities for Na^+, MA^+, EA^+,

the MDCK I-Venus-claudin-21 cell sheets compared to the MDCK I-Venus cell sheets (Fig. 2A, panel d; see Fig. S6A, panel a, in the supplemental material). These results indicate that claudin-21 increases the paracellular permeability not only for small cations, such as Na^+, MA^+, and EA^+ (diameter < 5 Å), but also for larger cations, such as TMA^+, TEA^+, Arg^+, and $NMDG^+$ (diameter > 5 Å).

Previous reports have shown that the paracellular passage across TJs is temperature dependent (12, 28, 31), and this property may depend on the molecular dynamics of the claudin-based TJ strands. Therefore, we assessed the temperature dependency of the paracellular permeability of MDCK I-Venus-claudin-21 cell sheets for small and large cations. The results showed that the paracellular permeabilities of the MDCK I-Venus-claudin-21 cell sheets for Na^+, MA^+, EA^+ TMA^+, TEA^+, Arg^+, and $NMDG^+$ were significantly decreased at 4°C compared to those at 37°C (Fig. 2B, panel a; see Fig. S6A, panel b, in the supplemental material). These data indicated that the claudin-21-based paracellular permeability was temperature dependent, presumably due to a decrease in the dynamics of claudin-21. It was thus possible that the claudin-21-based permeability at 4°C was caused by the formation of "cation-selective" and "size-restrictive" pores by this protein. Size exclusion analysis indicated that the approximate diameter of the paracellular pore of claudin-21 was 5.6 Å at 4°C (Fig. 2B, panel b).

Next, we assessed the temperature-dependent paracellular permeabilities of the MDCK I-Venus and MDCK I-Venus-claudin-21 cell sheets for various cations. The temperature-dependent permeabilities (the permeabilities at 37°C minus the permeabilities at 4°C) of the MDCK I-Venus-claudin-21 cell sheets for small and large cations were increased compared to those of the MDCK I-Venus cell sheets (Fig. 2B, panel d). We also found that the claudin-21-based paracellular permeability was proportional to the temperature (see Fig. S6B, panel a, in the supplemental material) and showed a preference for cations (see Fig. S6B, panel b). We further determined that claudin-21 contributed to the temperature-dependent paracellular permeability, with a size exclusion threshold of approximately 5.6 Å (Fig. 2B, panel e). These findings supported the idea that the temperature dependency of paracellular permeability was due to a change in the molecular dynamics of TJ strands (7, 19, 29), including the dynamics of paracellular channel formation.

These characteristics of claudin-21 were compared to those of claudin-15, which has been identified as a typical paracellular channel. For this purpose, we also examined the electrophysiological characterization of claudin-15's paracellular channel activity in stable transfectants of MDCK I cells expressing N-terminally Venus-tagged mouse claudin-15 (MDCK I-Venus-claudin-15 cells). The exogenous claudin-15 of MDCK I-Venus-claudin-15 cells was mainly colocalized with the TJ marker ZO-1 (Fig. 1B; see Fig. S4B in the supplemental material). The claudin-15 expression level of MDCK I-Venus-claudin-15 cells was high enough to decrease the TER (Fig. 2A, panel a), and the paracellular channel functions of this claudin were similar to those of claudin-21 in our MDCK I cell system. First, claudin-15 formed a cation-selective pore for Na^+ but not for Cl^- (Fig. 2A, panel b). Claudin-15 increased the paracellular permeability not only for small cations, such as Na^+, MA^+, and EA^+ (diameter <5 Å), but also for larger cations, such as TMA^+, TEA^+, Arg^+, and $NMDG^+$ (diameter >5 Å) (Fig. 2A, panel d). Furthermore, the claudin-15-based paracellular permeability was temperature dependent (Fig. 2B, panel a). The size exclusion analysis indicated that the approximate diameter of the paracellular pore of claudin-15 was 5.6 Å at 4°C (Fig. 2B, panel e). Finally, the temperature-dependent permeabilities (the permeabilities at 37°C minus the permeabilities at 4°C) of the MDCK I-Venus-claudin-15 cell sheets for small and large cations were increased compared to those of the MDCK I-Venus cell sheets (Fig. 2B, panel c), and the temperature-dependent paracellular permeability had a size exclusion threshold of approximately 5.6 Å (Fig. 2B, panel f).

Taken together, these data showed that claudin-21 forms cation-selective and size-restrictive paracellular pores for small cations, such as Na^+, and that it also regulates the cation-selective permeability for larger solutes, similarly to claudin-15. The paracellular functions of claudin-21 and -15 were temperature dependent, by a mechanism that is a subject for future study.

Structural analysis of the claudin-21-based paracellular pore. To verify claudin-21's ion selectivity, we built homology models of claudin-21 based on the crystal structure of claudin-15 (25). We also built structural models of claudin-2 and -10a, as channels with a preference for positively and negatively charged ions, respectively. The recently analyzed structure of claudin-15 revealed that the charge-selective passage across TJs depends on the charges of the residues in the extracellular domain. Mutation of the negatively charged residues Asp55 and Asp64, located on one edge of the β-sheet domain of claudin-15, to positively charged residues converts the ion selectivity to the opposite charge (10) (Fig. 3A and B, panels a and b). In addition to these residues, evidence suggests that residues on β3-β4 in other channel-forming claudins are essential for determining the charge selectivity of TJs (10). The distribution of the electrostatic potential at the extracellular surface of claudin-15 shows that half of the β-sheet domain forms a negatively charged "palm" (Fig. 3A and B, panels a and b). Our homology models also indicate that the cation-selective claudin-2 and the ion channel claudin-21 have similarly negatively charged surfaces, whereas the surface of anion-selective

TMA^+, TEA^+, Arg^+, and $NMDG^+$ of MDCK I-Venus, MDCK I-Venus-claudin-21, and MDCK I-Venus-claudin-15 cell sheets at 37°C ($n = 4$/group). Statistical analysis was performed on 2 sets of data from MDCK I-Venus and MDCK I-Venus-claudin-21 cells or MDCK I-Venus and MDCK I-Venus-claudin-15 cells. ***, $P < 0.001$. (B) (a) Transepithelial ion permeabilities for Na^+, MA^+, EA^+, TMA^+, TEA^+, Arg^+, and $NMDG^+$ of MDCK I-Venus, MDCK I-Venus-claudin-21, and MDCK I-Venus-claudin-15 cell sheets at 4°C ($n = 4$/group). Statistical analysis was performed on 2 sets of data from MDCK I-Venus and MDCK I-Venus-claudin-21 cells or MDCK I-Venus and MDCK I-Venus-claudin-15 cells. **, $P < 0.01$; ***, $P < 0.001$. (b) Estimation of the approximate diameter of claudin-21's pore (arrow). (c) Temperature-dependent paracellular permeabilities (permeabilities at 37°C minus permeabilities at 4°C) for Na^+, MA^+, EA^+, TMA^+, TEA^+, Arg^+, and $NMDG^+$ of MDCK I-Venus, MDCK I-Venus-claudin-21, and MDCK I-Venus-claudin-15 cell sheets ($n = 4$/group). Statistical analysis was performed on 2 sets of data from MDCK I-Venus and MDCK I-Venus-claudin-21 cells or MDCK I-Venus and MDCK I-Venus-claudin-15 cells. ***, $P < 0.001$. (d) Estimation of the size exclusion threshold of the temperature-dependent paracellular permeability due to claudin-21 (arrow). (e) Estimation of the approximate diameter of claudin-15's pore (arrow). (f) Estimation of the size exclusion threshold of the temperature-dependent paracellular permeability due to claudin-15 (arrow).

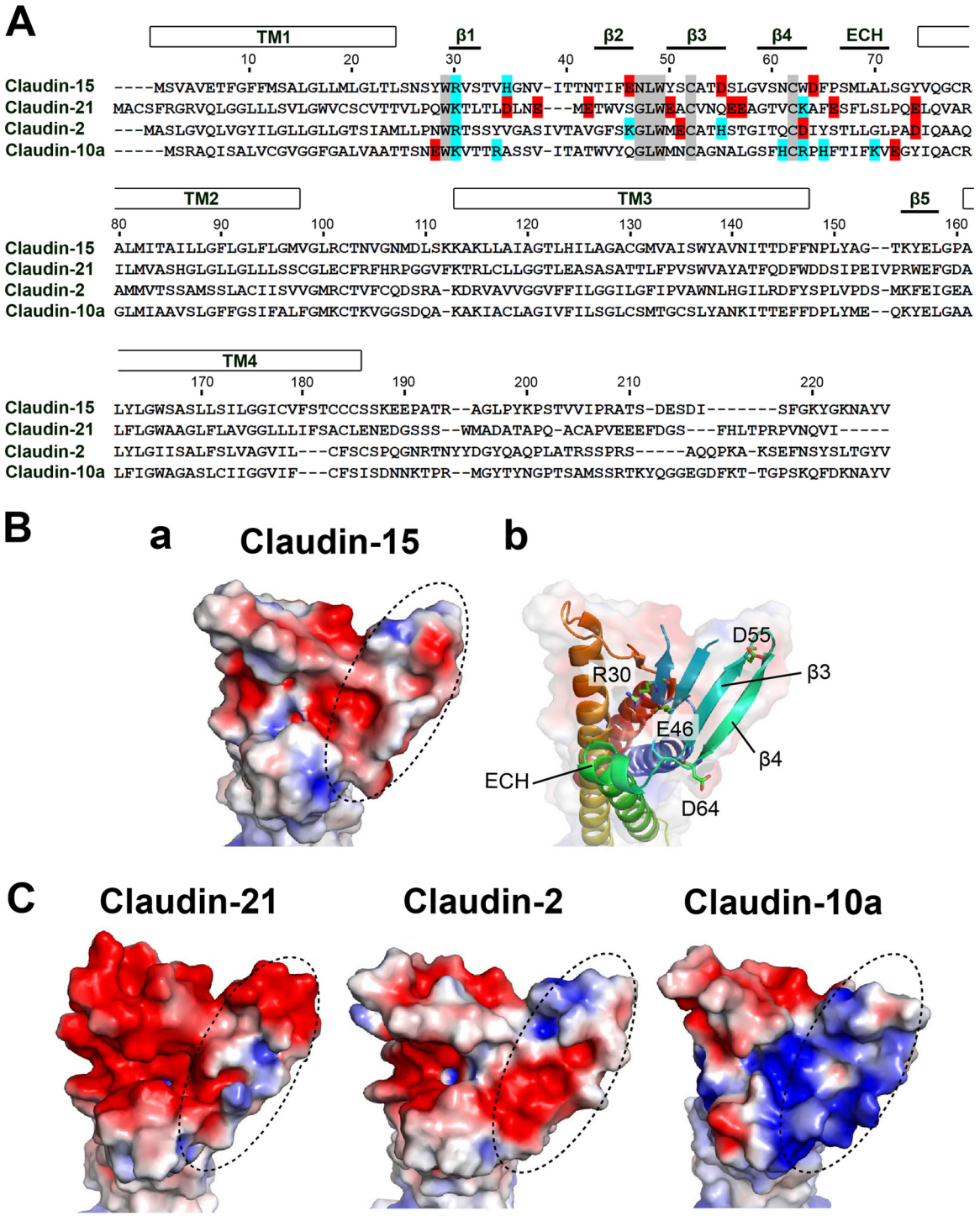

FIG 3 Structural analysis of the claudin-21-based paracellular pore. (A) Alignment of the amino acid sequences of paracellular channel-type mouse claudins, including claudin-21. Numbers at the top indicate the amino acid positions of mouse claudin-15. Negatively and positively charged amino acids in the first extracellular segment are shown in red and blue, respectively. Representative claudin motifs are shown in gray. (B) (a) Electrostatic potential of the claudin-15 surface contoured from −2 *kT/e* (red) to +2 *kT/e* (blue). (b) Ribbon representation of claudin-15 with a transparent surface and viewed from the same direction as in panel a, with color changes from the N terminus (blue) to the C terminus (red). (C) Electrostatic potential surfaces of the extracellular domains of homology models (claudin-2, -21, and -10a), viewed as in panel B. Dashed ovals indicate the β3-β4 region, where residues important for charge selectivity of the paracellular channel are located.

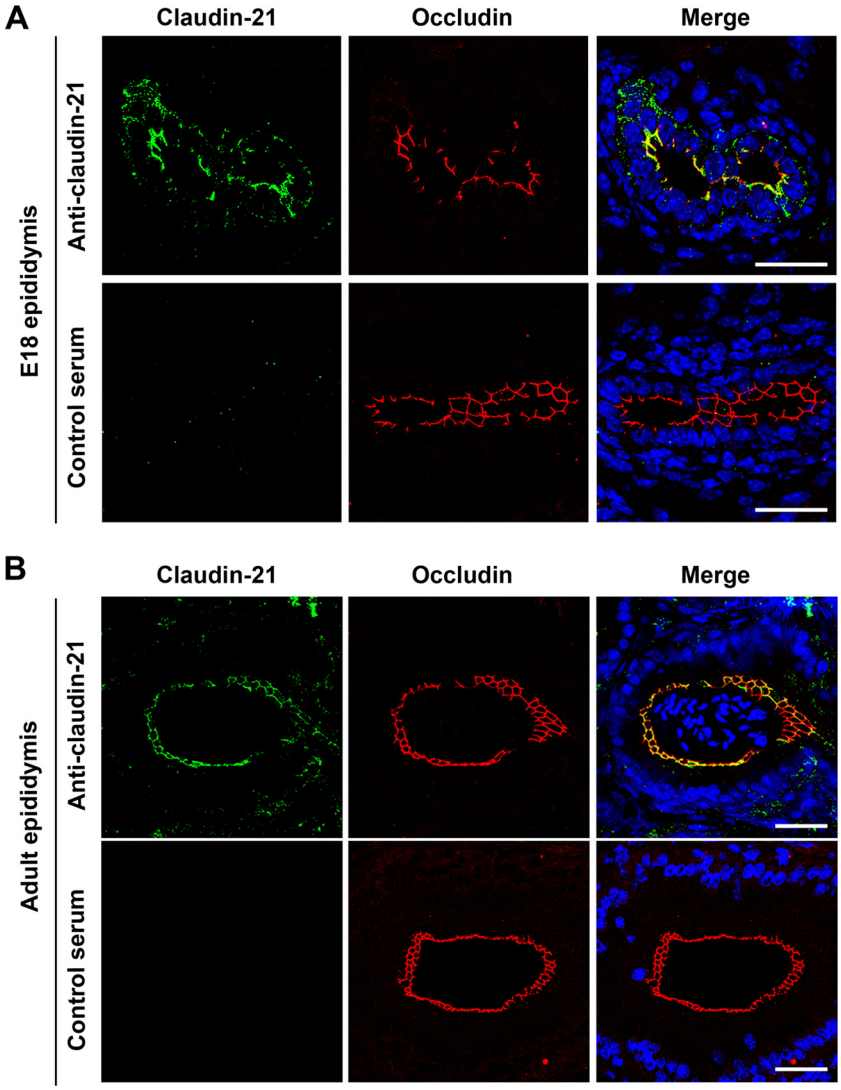

FIG 4 Claudin-21 expression in mouse tissues. Immunofluorescence micrographs show epididymides from an E18 mouse (A) and an adult mouse (B) costained with an anti-claudin-21 pAb and an antioccludin MAb or with antiserum and an antioccludin MAb. DAPI (4′,6-diamidino-2-phenylindole) was used to detect nuclei. The anti-claudin-21- or antiserum-positive signals (green), the antioccludin-positive signals (red), and nuclei (blue) are shown. Bars, 50 μm.

claudin-10a is positively charged (Fig. 3C). These surface distributions of the electrostatic potential help to explain the permeability preference of claudin-21 for Na^+ rather than Cl^-. In particular, it has been suggested that the grooves in the specific palm region of all the strands from β1 to β5 form a paracellular ion pathway that contributes to claudins' ion selectivity (25).

Claudin-21 expression *in vivo*. To confirm claudin-21's expression *in vivo*, we examined the mRNA expression of claudin-21 in several tissues of E18.5 and adult mice by probe-based qRT-PCR. We detected a high level of claudin-21 mRNA expression in the testis with epididymis of the E18.5 mice (see Fig. S7A in the supplemental material). We found by immunofluorescence assay that claudin-21 was expressed in the epididymis but not in the testis in E18 mice and colocalized with the tight junctional markers occludin (Fig. 4A) and ZO-1 (see Fig. S7B and C, panel a). We detected the signal for claudin-21 in the adult mouse epididymis but not in the testis, and the signal was colocalized with the tight junctional marker occludin (Fig. 4B; see Fig. S7C, panel b). To validate the quite low claudin-21 mRNA expression in several tissues other than the E18.5 testis and/or epididymis (Fig. 4A), we carried out 3′RACE using RNAs from fetal mouse liver (see Fig. S8A). This method was suitable for the detection of the quite small amount of claudin-21 mRNA because this method verified amplification from claudin-21 mRNA but not from genomic DNA. The claudin-21 3′RACE products indicated the presence of mature claudin-21 mRNA with a poly(A) tail following the AATAAA sequence (see Fig. S8B). These findings revealed that claudin-21 mRNA is expressed *in vivo*, as previously reported (8), and that claudin-21 resides in the TJ strands *in vivo*.

DISCUSSION

New classification of claudin-21 as a paracellular channel-type claudin. Here we identified claudin-21 as a paracellular channel-type claudin. Although we could show that MDCK I cells, which are canine cells, expressed at least claudin-1, -3, -4, -7, -14, and -19, well-characterized RT-PCR-appropriate primer sets or anti-

bodies are not available for all 27 canine claudins. However, given that claudin-21's effect on MDCK I cell permeability was significant and was similar to the effects of claudin-2 and -15, which are representative paracellular channel-type claudins, we conclude that claudin-21 is a paracellular channel-type claudin.

Characterization of the claudin-21-based pore in the paracellular channel. In the present study, we electrophysiologically determined that claudin-21 forms a charge-selective and size-restrictive pore for small cations. The recently determined structure of claudin-15, analyzed by X-ray crystallography at a 2.4-Å resolution, indicates that the paracellular pathway is formed by the claudin's extracellular domain (25, 26). The surface distribution of the electrostatic potential at claudin-21's pore region has a negative charge, which would cause its pore to be attractive for cations but repulsive for anions. Together with our experimental results, this electrostatic surface distribution supports our assignment of claudin-21 as a paracellular channel showing a preference for cations. With regard to the paracellular permeation of Na^+, the most abundant cation in the body, the physiologically estimated diameter of claudin-21's pore (~5.6 Å) is smaller than the diameter of hydrated Na^+ (7.2 Å) (39). To pass through the claudin-21-based channel, Na^+ might be partially dehydrated, similar to the case for claudin-2-based channels (~6.5 Å) (31). Moreover, evidence suggests that claudin-2 mediates paracellular water flow as well as ion permeation (24). Further comparative analyses of these channel-forming claudins will help to clarify their specific functions in biological systems.

Temperature dependence of claudin-21-based paracellular permeability. In the present study, exogenously expressed claudin-21 showed temperature-dependent paracellular permeabilities for both small and larger cations. It was previously reported that the typical paracellular channel-type claudin-2 also has a temperature-dependent paracellular permeability for small cations (12, 31). Considering that claudins polymerize to form the TJ strands, it seems reasonable that the paracellular pathway, including the pore formation of paracellular channels, is not static but is dynamically regulated, consistent with its temperature dependency. In this respect, few studies of the dynamic behaviors of TJ strands and TJ proteins have been reported (27, 29, 40). Further quantitative analyses of the relationship between the molecular dynamics of claudins and paracellular permeability are required to clarify the regulation of the paracellular pathway.

General aspects of paracellular channel claudins. Although we propose here that claudin-21 is a channel-type claudin, its expression pattern and relatively low endogenous level suggest that it functions in a restricted set of tissues (8). The expression of claudin-21 is high during embryonic stages, although its expression persists at low levels in the adult. This developmental expression pattern suggests that claudin-21 has morphogenetic functions. Future analyses of the embryonic stage-specific functions of the paracellular channel-type claudin-21 will provide insight about the regulation of microenvironments in developing biological systems.

The systematic characterization of each claudin has provided insight into the formation and regulation of leaky and tight TJs *in vitro* and *in vivo*. The *in vivo* analysis of knockout mice has also provided useful information about the physiological roles of claudins. For example, a recent mouse study revealed that claudin-2 and -15 have paracellular cation channel activity in the small intestine, elucidating the molecular players that determine the paracellular channel function in this organ. These claudins were found to be required for the paracellular flow of sodium ions into the lumen for the absorption of glucose, amino acids, and bile acids, which are required for lipid digestion (17, 20).

The physiological roles of the paracellular permeability for large solutes have not been clarified. However, pathophysiological roles have been reported for some claudin knockout mice. For example, the loss of claudin-5 increases the paracellular permeability for large solutes across TJs between endothelial cells in the brain (41). In addition, the intestine-specific loss of claudin-7, which increases the paracellular permeability for the intestinal microbiota-derived chemotactic peptide fMLP across colonic epithelial cell sheets, specifically causes colonic inflammation (22). These findings suggest that the paracellular permeability for various solutes is specifically regulated by the TJ strands to maintain biological systems.

Although the expression and roles of these relatively abundant claudins have gradually been uncovered, much less is known about the roles of the less abundant, cell-type-specific claudins. Claudins expressed at low levels or in only a few tissues or sites are likely to be involved in the fine regulation of tissue function-specific homeostasis. Additional functional analyses of these systems will shed light on the importance of compartmentalization and the formation and regulation of homeostasis in specific biological systems.

Our present findings indicate that further analyses of claudin-21-based TJs may help to elucidate the molecular mechanisms underlying the paracellular permeability for variously sized solutes. Further investigation of this protein may help to reveal how paracellular pathways are precisely controlled.

ACKNOWLEDGMENTS

We thank the members of our laboratories, especially Tomoki Yano for discussions, Masami Uji and Asuka Hagiwara for technical assistance, and Grace Gray and Leslie Miglietta for reading the manuscript.

This work was supported in part by Grants-in-Aid for Scientific Research (A) and Creative Scientific Research from the Ministry of Education, Culture, Sports, Science and Technology of Japan (MEXT) and from CREST (Core Research for Evolutional Science and Technology) of the Japan Science and Technology Agency (JST) to Sachiko Tsukita and by Grants-in-Aid for Scientific Research from MEXT and from the Research and Development Program for New Bio-Industry Initiatives to Kosei Takeuchi. This research was also supported by Grants-in-Aid for Scientific Research (S) to Yoshinori Fujiyoshi, Grants-in-Aid for Scientific Research (C) to Kazutoshi Tani, and grants from the Japan New Energy and Industrial Technology Development Organization (NEDO) and the National Institute of Biomedical Innovation to Yoshinori Fujiyoshi.

FUNDING INFORMATION

Ministry of Education, Culture, Sports, Science, and Technology (MEXT) provided funding to Sachiko Tsukita under grant number 24247037. Ministry of Education, Culture, Sports, Science, and Technology (MEXT) provided funding to Yoshinori Fujiyoshi under grant number 22227004. Ministry of Education, Culture, Sports, Science, and Technology (MEXT) provided funding to Kazutoshi Tani under grant number 26440024. Ministry of Education, Culture, Sports, Science, and Technology (MEXT) provided funding to Kosei Takeuchi. Core Research for Evolutional Science and Technology, Japan Science and Technology Agency (CREST, JST) provided funding to Sachiko Tsukita.

The funders had no role in study design, data collection and interpretation, or the decision to submit the work for publication.

REFERENCES

1. **Franke WW.** 2009. Discovering the molecular components of intercellular junctions—a historical view. Cold Spring Harb Perspect Biol **1:**a003061. http://dx.doi.org/10.1101/cshperspect.a003061.
2. **Tsukita S, Furuse M, Itoh M.** 2001. Multifunctional strands in tight junctions. Nat Rev Mol Cell Biol **2:**285–293. http://dx.doi.org/10.1038/35067088.
3. **Van Itallie CM, Anderson JM.** 2006. Claudins and epithelial paracellular transport. Annu Rev Physiol **68:**403–429. http://dx.doi.org/10.1146/annurev.physiol.68.040104.131404.
4. **Anderson JM, Van Itallie CM.** 2009. Physiology and function of the tight junction. Cold Spring Harb Perspect Biol **1:**a002584. http://dx.doi.org/10.1101/cshperspect.a002584.
5. **Tsukita S, Yamazaki Y, Katsuno T, Tamura A, Tsukita S.** 2008. Tight junction-based epithelial microenvironment and cell proliferation. Oncogene **27:**6930–6938. http://dx.doi.org/10.1038/onc.2008.344.
6. **Amasheh S, Milatz S, Krug SM, Markov AG, Gunzel D, Amasheh M, Fromm M.** 2009. Tight junction proteins as channel formers and barrier builders. Ann N Y Acad Sci **1165:**211–219. http://dx.doi.org/10.1111/j.1749-6632.2009.04439.x.
7. **Shen L, Weber CR, Raleigh DR, Yu D, Turner JR.** 2011. Tight junction pore and leak pathways: a dynamic duo. Annu Rev Physiol **73:**283–309. http://dx.doi.org/10.1146/annurev-physiol-012110-142150.
8. **Mineta K, Yamamoto Y, Yamazaki Y, Tanaka H, Tada Y, Saito K, Tamura A, Igarashi M, Endo T, Takeuchi K, Tsukita S.** 2011. Predicted expansion of the claudin multigene family. FEBS Lett **585:**606–612. http://dx.doi.org/10.1016/j.febslet.2011.01.028.
9. **Furuse M, Furuse K, Sasaki H, Tsukita S.** 2001. Conversion of zonulae occludentes from tight to leaky strand type by introducing claudin-2 into Madin-Darby canine kidney I cells. J Cell Biol **153:**263–272. http://dx.doi.org/10.1083/jcb.153.2.263.
10. **Colegio OR, Van Itallie CM, McCrea HJ, Rahner C, Anderson JM.** 2002. Claudins create charge-selective channels in the paracellular pathway between epithelial cells. Am J Physiol Cell Physiol **283:**C142–C147. http://dx.doi.org/10.1152/ajpcell.00038.2002.
11. **Van Itallie CM, Fanning AS, Anderson JM.** 2003. Reversal of charge selectivity in cation or anion-selective epithelial lines by expression of different claudins. Am J Physiol Renal Physiol **285:**F1078–F1084. http://dx.doi.org/10.1152/ajprenal.00116.2003.
12. **Yu AS, Enck AH, Lencer WI, Schneeberger EE.** 2003. Claudin-8 expression in Madin-Darby canine kidney cells augments the paracellular barrier to cation permeation. J Biol Chem **278:**17350–17359. http://dx.doi.org/10.1074/jbc.M213286200.
13. **Alexandre MD, Lu Q, Chen YH.** 2005. Overexpression of claudin-7 decreases the paracellular Cl^- conductance and increases the paracellular Na^+ conductance in LLC-PK1 cells. J Cell Sci **118:**2683–2693. http://dx.doi.org/10.1242/jcs.02406.
14. **Hou J, Gomes AS, Paul DL, Goodenough DA.** 2006. Study of claudin function by RNA interference. J Biol Chem **281:**36117–36123. http://dx.doi.org/10.1074/jbc.M608853200.
15. **Hou J, Renigunta A, Gomes AS, Hou M, Paul DL, Waldegger S, Goodenough DA.** 2009. Claudin-16 and claudin-19 interaction is required for their assembly into tight junctions and for renal reabsorption of magnesium. Proc Natl Acad Sci U S A **106:**15350–15355. http://dx.doi.org/10.1073/pnas.0907724106.
16. **Muto S, Hata M, Taniguchi J, Tsuruoka S, Moriwaki K, Saitou M, Furuse K, Sasaki H, Fujimura A, Imai M, Kusano E, Tsukita S, Furuse M.** 2010. Claudin-2-deficient mice are defective in the leaky and cation-selective paracellular permeability properties of renal proximal tubules. Proc Natl Acad Sci U S A **107:**8011–8016. http://dx.doi.org/10.1073/pnas.0912901107.
17. **Tamura A, Hayashi H, Imasato M, Yamazaki Y, Hagiwara A, Wada M, Noda T, Watanabe M, Suzuki Y, Tsukita S.** 2011. Loss of claudin-15, but not claudin-2, causes Na^+ deficiency and glucose malabsorption in mouse small intestine. Gastroenterology **140:**913–923. http://dx.doi.org/10.1053/j.gastro.2010.08.006.
18. **Breiderhoff T, Himmerkus N, Stuiver M, Mutig K, Will C, Meij IC, Bachmann S, Bleich M, Willnow TE, Muller D.** 2012. Deletion of claudin-10 (Cldn10) in the thick ascending limb impairs paracellular sodium permeability and leads to hypermagnesemia and nephrocalcinosis. Proc Natl Acad Sci U S A **109:**14241–14246. http://dx.doi.org/10.1073/pnas.1203834109.
19. **Gunzel D, Yu AS.** 2013. Claudins and the modulation of tight junction permeability. Physiol Rev **93:**525–569. http://dx.doi.org/10.1152/physrev.00019.2012.
20. **Wada M, Tamura A, Takahashi N, Tsukita S.** 2013. Loss of claudins 2 and 15 from mice causes defects in paracellular Na^+ flow and nutrient transport in gut and leads to death from malnutrition. Gastroenterology **144:**369–380. http://dx.doi.org/10.1053/j.gastro.2012.10.035.
21. **Matsumoto K, Imasato M, Yamazaki Y, Tanaka H, Watanabe M, Eguchi H, Nagano H, Hikita H, Tatsumi T, Takehara T, Tamura A, Tsukita S.** 2014. Claudin 2 deficiency reduces bile flow and increases susceptibility to cholesterol gallstone disease in mice. Gastroenterology **147:**1134.e10–1145.e10. http://dx.doi.org/10.1053/j.gastro.2014.07.033.
22. **Tanaka H, Takechi M, Kiyonari H, Shioi G, Tamura A, Tsukita S.** 2015. Intestinal deletion of Claudin-7 enhances paracellular organic solute flux and initiates colonic inflammation in mice. Gut **64:**1529–1538. http://dx.doi.org/10.1136/gutjnl-2014-308419.
23. **Amasheh S, Meiri N, Gitter AH, Schoneberg T, Mankertz J, Schulzke JD, Fromm M.** 2002. Claudin-2 expression induces cation-selective channels in tight junctions of epithelial cells. J Cell Sci **115:**4969–4976. http://dx.doi.org/10.1242/jcs.00165.
24. **Rosenthal R, Milatz S, Krug SM, Oelrich B, Schulzke JD, Amasheh S, Gunzel D, Fromm M.** 2010. Claudin-2, a component of the tight junction, forms a paracellular water channel. J Cell Sci **123:**1913–1921. http://dx.doi.org/10.1242/jcs.060665.
25. **Suzuki H, Nishizawa T, Tani K, Yamazaki Y, Tamura A, Ishitani R, Dohmae N, Tsukita S, Nureki O, Fujiyoshi Y.** 2014. Crystal structure of a claudin provides insight into the architecture of tight junctions. Science **344:**304–307. http://dx.doi.org/10.1126/science.1248571.
26. **Suzuki H, Tani K, Tamura A, Tsukita S, Fujiyoshi Y.** 2015. Model for the architecture of claudin-based paracellular ion channels through tight junctions. J Mol Biol **427:**291–297. http://dx.doi.org/10.1016/j.jmb.2014.10.020.
27. **Shen L, Weber CR, Turner JR.** 2008. The tight junction protein complex undergoes rapid and continuous molecular remodeling at steady state. J Cell Biol **181:**683–695. http://dx.doi.org/10.1083/jcb.200711165.
28. **Tomita M, Menconi MJ, Delude RL, Fink MP.** 2000. Polarized transport of hydrophilic compounds across rat colonic mucosa from serosa to mucosa is temperature dependent. Gastroenterology **118:**535–543. http://dx.doi.org/10.1016/S0016-5085(00)70259-9.
29. **Sasaki H, Matsui C, Furuse K, Mimori-Kiyosue Y, Furuse M, Tsukita S.** 2003. Dynamic behavior of paired claudin strands within apposing plasma membranes. Proc Natl Acad Sci U S A **100:**3971–3976. http://dx.doi.org/10.1073/pnas.0630649100.
30. **Gunzel D, Stuiver M, Kausalya PJ, Haisch L, Krug SM, Rosenthal R, Meij IC, Hunziker W, Fromm M, Muller D.** 2009. Claudin-10 exists in six alternatively spliced isoforms that exhibit distinct localization and function. J Cell Sci **122:**1507–1517. http://dx.doi.org/10.1242/jcs.040113.
31. **Yu AS, Cheng MH, Angelow S, Gunzel D, Kanzawa SA, Schneeberger EE, Fromm M, Coalson RD.** 2009. Molecular basis for cation selectivity in claudin-2-based paracellular pores: identification of an electrostatic interaction site. J Gen Physiol **133:**111–127. http://dx.doi.org/10.1085/jgp.200810154.
32. **Thompson JD, Higgins DG, Gibson TJ.** 1994. CLUSTAL W: improving the sensitivity of progressive multiple sequence alignment through sequence weighting, position-specific gap penalties and weight matrix choice. Nucleic Acids Res **22:**4673–4680. http://dx.doi.org/10.1093/nar/22.22.4673.
33. **Sali A, Blundell TL.** 1993. Comparative protein modelling by satisfaction of spatial restraints. J Mol Biol **234:**779–815. http://dx.doi.org/10.1006/jmbi.1993.1626.
34. **Emsley P, Lohkamp B, Scott WG, Cowtan K.** 2010. Features and development of Coot. Acta Crystallogr D Biol Crystallogr **66:**486–501. http://dx.doi.org/10.1107/S0907444910007493.
35. **Brunger AT, Adams PD, Clore GM, DeLano WL, Gros P, Grosse-Kunstleve RW, Jiang JS, Kuszewski J, Nilges M, Pannu NS, Read RJ, Rice LM, Simonson T, Warren GL.** 1998. Crystallography & NMR system: a new software suite for macromolecular structure determination. Acta Crystallogr D Biol Crystallogr **54:**905–921.
36. **Baker NA, Sept D, Joseph S, Holst MJ, McCammon JA.** 2001. Electrostatics of nanosystems: application to microtubules and the ribosome. Proc Natl Acad Sci U S A **98:**10037–10041. http://dx.doi.org/10.1073/pnas.181342398.

37. **Lal-Nag M, Morin PJ.** 2009. The claudins. Genome Biol **10:**235. http://dx.doi.org/10.1186/gb-2009-10-8-235.
38. **Katoh M, Katoh M.** 2003. CLDN23 gene, frequently down-regulated in intestinal-type gastric cancer, is a novel member of CLAUDIN gene family. Int J Mol Med **11:**683–689.
39. **Nightingale ER.** 1959. Phenomenological theory of ion solution—effective radii of hydrated ions. J Phys Chem A **63:**1381–1387. http://dx.doi.org/10.1021/j150579a011.
40. **Yamazaki Y, Tokumasu R, Kimura H, Tsukita S.** 2011. Role of claudin species-specific dynamics in reconstitution and remodeling of the zonula occludens. Mol Biol Cell **22:**1495–1504. http://dx.doi.org/10.1091/mbc.E10-12-1003.
41. **Nitta T, Hata M, Gotoh S, Seo Y, Sasaki H, Hashimoto N, Furuse M, Tsukita S.** 2003. Size-selective loosening of the blood-brain barrier in claudin-5-deficient mice. J Cell Biol **161:**653–660. http://dx.doi.org/10.1083/jcb.200302070.